SUPPORTING INFORMATION

# Hybrid Carbon Dot Assembly as a Reactive Oxygen Species Nanogenerator for Ultrasound-Assisted Tumor Ablation

*Deblin Jana,[†] Dongdong Wang,[†] Praveenbalaji Rajendran,[‡] Anivind Kaur Bindra,[†] Yi Guo,[†] Jiawei Liu,[†] Manojit Pramanik,[‡] Yanli Zhao*[,†,‡]*

[†]Division of Chemistry and Biological Chemistry, School of Physical and Mathematical Sciences, Nanyang Technological University, 21 Nanyang Link, Singapore 637371, Singapore. [‡]School of Chemical and Biomedical Engineering, Nanyang Technological University, 62 Nanyang Drive, Singapore 637459, Singapore.

E-mail: zhaoyanli@ntu.edu.sg

**Reagents and materials.** All chemicals and solvents were utilized as received without any additional purification. Copper(II) acetylacetonate ($Cu(acac)_2$), IR-780 iodide, and molybdenum dichloride dioxide ($MoO_2Cl_2$) were purchased from Sigma-Aldrich (Singapore). DSPE-PEG2000 was purchased from Avanti Polar Lipids, Inc. (USA). 3-(4,5-Dimethylthiazol-2-yl)-2,5-diphenyltetrazolium bromide (MTT) was purchased from Tokyo Chemical Industry. Murine breast cancer cells (4T1) were obtained from American Type Culture Collection (ATCC). Deionized water (DI water, 18.2 MΩ·cm resistivity at 25 °C) was used throughout the entire experiments.

**Measurements.** Transmission electron microscopy (TEM) images were collected by a JEOL JEM 2100plus microscopy at an accelerating voltage of 200 kV. Scanning electron microscopy (SEM) images were measured on a JEOL JSM-6700M (Japan) microscopy. Ultraviolet-visible (UV-vis) absorption spectra were measured on a Shimadzu UV-3600 spectrometer. X-Ray photoelectron spectroscopy (XPS) was performed with a monochromatic Mg X-ray radiation source in a Phoibos 100 spectrometer (SPECS, Germany). Fourier transformed infrared (FTIR) spectra were measured on a Shimadzu IR Prestige-21 FTIR spectrometer. Confocal laser scanning microscopy images were acquired by ZEISS LSM 800 microscopy. Flow cytometry was taken on Guava EasyCyte 6-2L cytometer. For measurements of ζ-potential and size distribution, a DLS instrument (Nano ZS ZEN3600, Malvern) was used. The quantitative elemental composition was determined by inductively coupled plasma optical emission spectrometry (ICP-OES, ELAN-DRCe, PerkinElmer). All the animal experiments were performed following the university laboratory animal guidelines from the Nanyang Technological University Institutional Animal Care and Use Committee (NTU-IACUC), with protocol number of A19016. Ultrasound (US) was used by following the specification unless mentioned: 1 MHz, 50% duty cycle.

**Intracellular •OH detection assay.** •OH generation inside cells under US irradiation was detected using coumarin-3-carboxylic acid assay and 3′-(p-Hydroxyphenyl) fluorescein (HPF) assay. 4T1 cells ($1 \times 10^5$ cells/well) were seeded on coverslips in a six-well plate and then incubated at 37 °C in the dark for 24 h. The medium was replaced with complete RPMI containing CMIR-CDa, MIR-CDa, or IR-CDa. After the incubation for 6 h, indicator solution was added by following the standard protocol. After the incubation for additional 10 min, cells were washed thrice with PBS. The cells were irradiated by US (2 min, 0.5 W $cm^{-2}$). PBS was used to wash the treated cells, and fluorescence images of the cells were attained under a confocal laser scanning microscope (Carl Zeiss LSM 800).

**Intracellular $^1O_2$ detection assay.** $^1O_2$ generation inside cells under US irradiation was detected using the SOSG assay. 4T1 cells ($1 \times 10^5$ cells/well) were seeded on coverslips in a six-well plate and then incubated at 37 °C in the dark for 24 h. The medium was replaced with complete RPMI containing CMIR-CDa, MIR-CDa, or IR-CDa. After the incubation for 6 h, SOSG (1 μM) was added. After incubation of 30 min, cells were washed thrice with PBS. Then, they were irradiated with US (2 min, 0.5 W $cm^{-2}$). PBS was used to wash the treated cells and fluorescence images of the cells were attained under a confocal laser scanning microscope (Carl Zeiss LSM 800).

**Intracellular $O_2^{\bullet-}$ and total ROS detection assay.** $O_2^{\bullet-}$ generation and total ROS inside cells under US irradiation were detected using the ROS/superoxide detection assay kit (ab139476, abcam). 4T1 cells ($1 \times 10^5$ cells/well) were seeded on coverslips in a six-well plate and then incubated at 37 °C in the dark for 24 h. The medium was replaced with complete RPMI containing CMIR-CDa, MIR-CDa, or IR-CDa. After the incubation for 6 h, ROS/superoxide detection assay was added by following the standard protocol given by the supplier. After incubation of 30 min, cells were washed thrice with PBS. Then, they were irradiated with US (2 min, 0.5 W $cm^{-2}$). PBS was used to wash the treated cells and fluorescence images of the cells were attained under a confocal laser scanning microscope (Carl Zeiss LSM 800).

**NIR-I photoacoustic tomography system.** Photoacoustic characterization was conducted on a home-made NIR-I photoacoustic tomography system. A 1064 nm Nd:YAG pulse (5 ns, 10 Hz) laser (Continuum, Surelite Ex) was utilized as the excitation source. Briefly, the 700 nm beam was directed to the single-ultrasound transducer (UST, V323-SU/2.25 MHz, Olympus NDT) scanner, and expanded by an optical diffuser to the inspection area. Water was utilized as the medium and UST was immersed in water to couple the acoustic signal to the transducer. The collected photoacoustic signals were then amplified and band-pass filtered (1–10 MHz) by ultrasound receiver unit (Olympus NDT, 5072PR). Later, photoacoustic signals were subsequently transmitted to a computer with a data acquisition card (25 Ms/s, GaGe, compuscope 4227) for digitalization and recording. Photoacoustic images of samples or mice were reconstructed *via* a delay-and-sum back projection algorithm. For *in vivo* photoacoustic tomography, balb/c mice bearing 4T1-xenograft tumor were anesthetized and administered with CMIR-CDa *via* tail vein injection. Photoacoustic images were captured at designated time points before and after the sample administration.

**Biochemical analysis of blood**. Mice without tumor (n = 3) were treated with PBS or CMIR-CDa through intravenous injection. At day 14 after the injection, blood samples were collected. For blood routine analysis, parameters such as white blood cell (WBC), red blood cells (RBC),

hemoglobin (HGB), hematocrit (PCV), mean corpuscular volume (MCV), mean corpuscular hemoglobin (MCH), mean corpuscular hemoglobin concentration (MCHC), platelets (PLT), and red cell distribution width (RDW) were measured. For blood biochemistry test, alkaline phosphatase (ALP), aspartate aminotransferase (AST), and blood urea nitrogen (BUN) serving as hepatic and renal function markers were measured.

**Statistical analysis**. All data were expressed as mean ± standard error of the mean. Statistical differences between two groups were calculated by two-tailed Student's t-test using GraphPad Prism 8.0 (GraphPad Software, Inc., CA, USA), and $p < 0.05$ was considered to be statistically significant. Asterisk (*) denotes statistical significance between bars (*$p < 0.05$, **$p < 0.01$, ***$p < 0.001$).

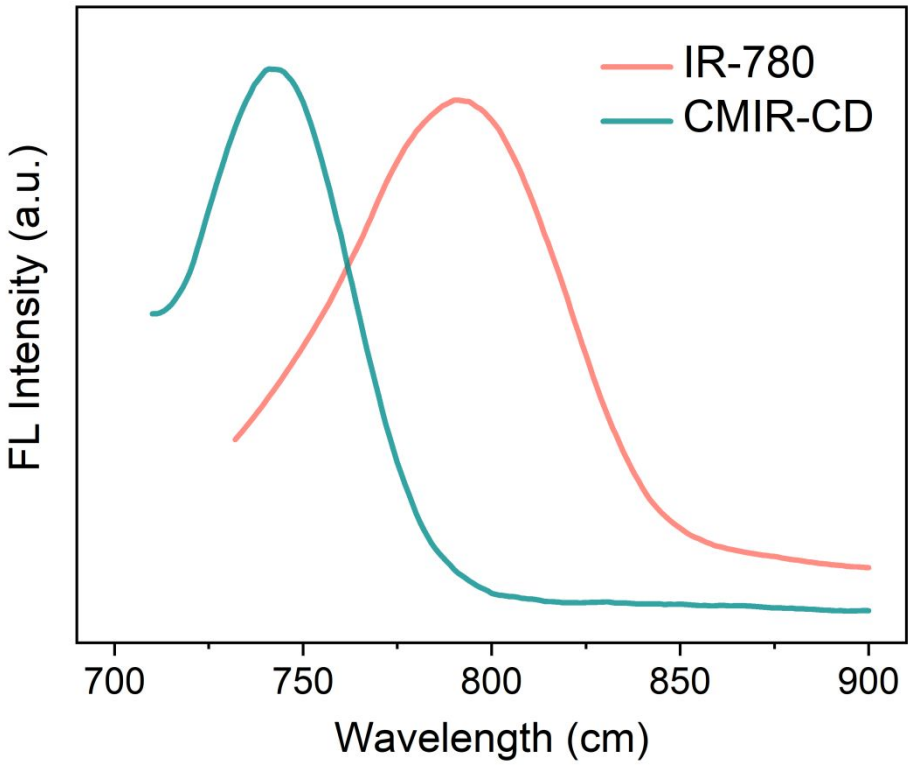


**Figure S1.** Emission spectra of CMIR-CD and IR-780 iodide in ethanol. FL: Fluorescence.

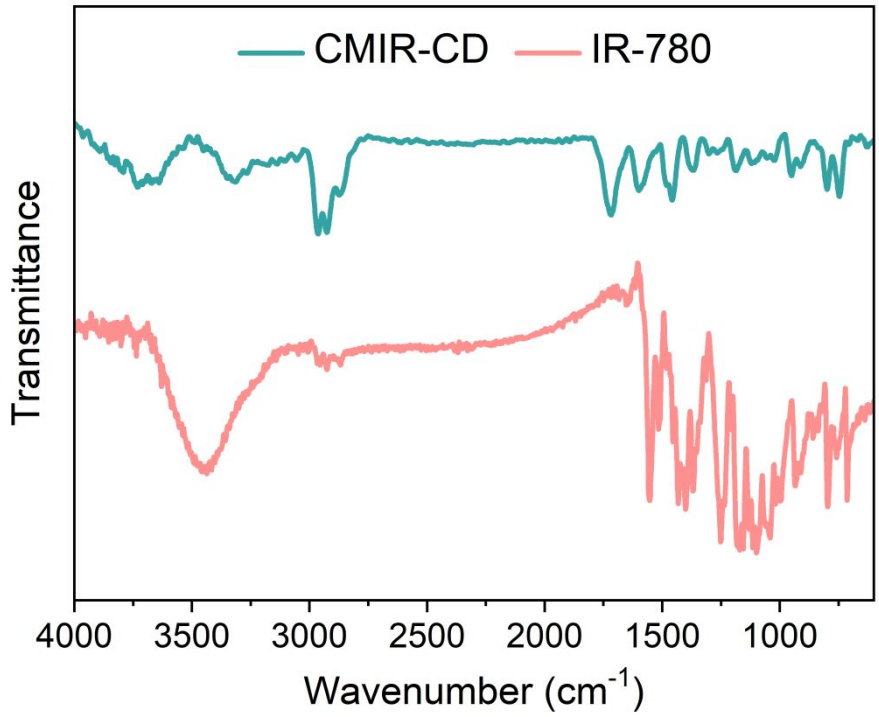


**Figure S2.** FTIR spectra of CMIR-CD and IR-780 iodide.

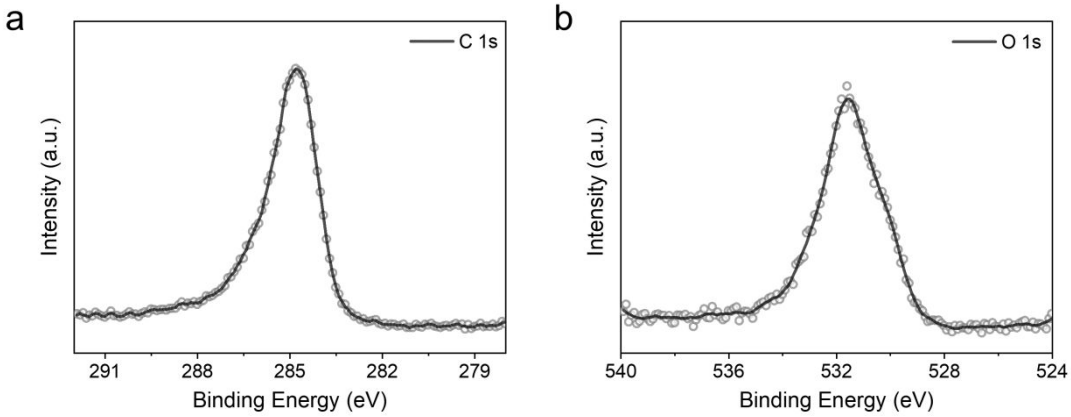


**Figure S3.** High resolution XPS analysis of a) C1s and b) O1s for CMIR-CD.

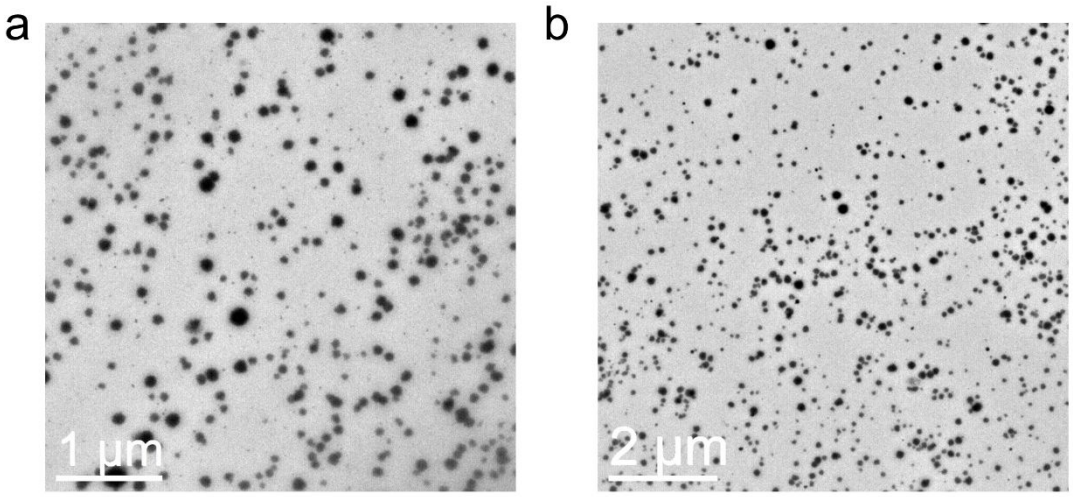


**Figure S4.** TEM images of a) MIR-CDa and b) IR-CDa.

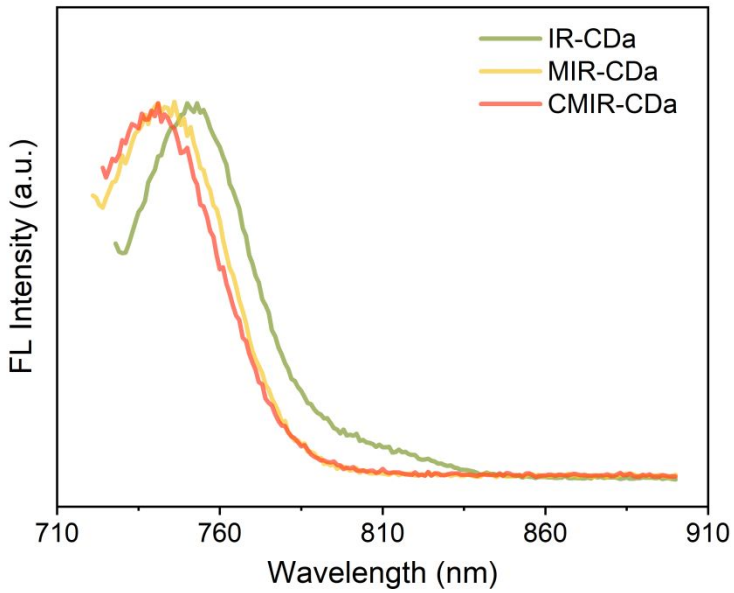


**Figure S5.** Emission spectra of IR-CDa, MIR-CDa and CMIR-CDa. FL: Fluorescence.

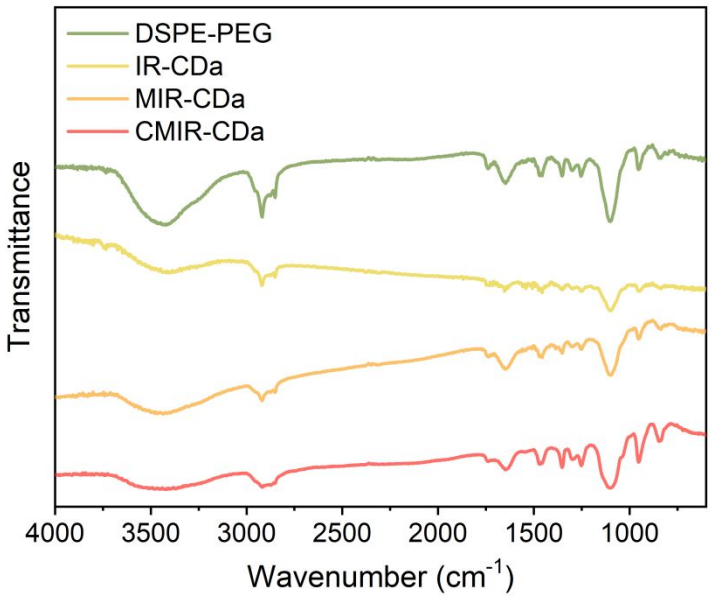


**Figure S6.** FTIR spectra of DSPE-PEG, IR-CDa, MIR-CDa, and CMIR-CDa.

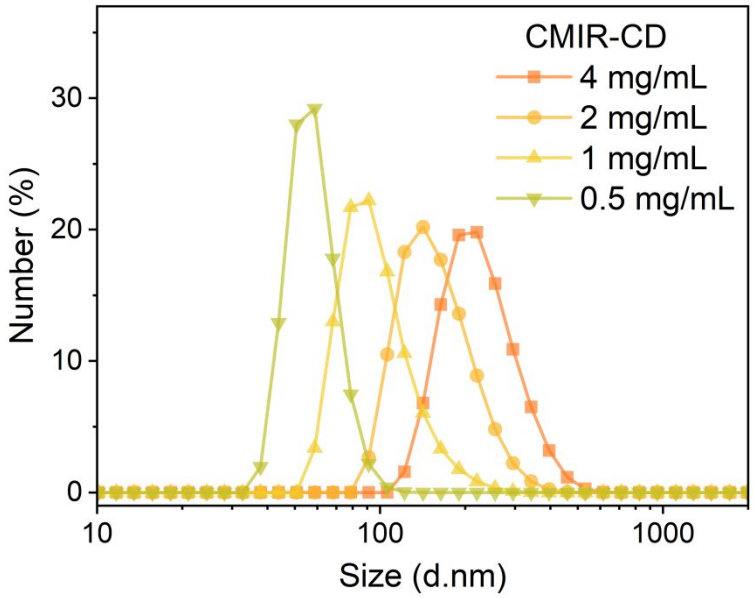


**Figure S7.** DLS curves of different CMIR-CDa formulations prepared from DSPE-PEG (5 mL, 2 mg/mL) and CMIR-CD (1 mL) with varying concentrations indicated.

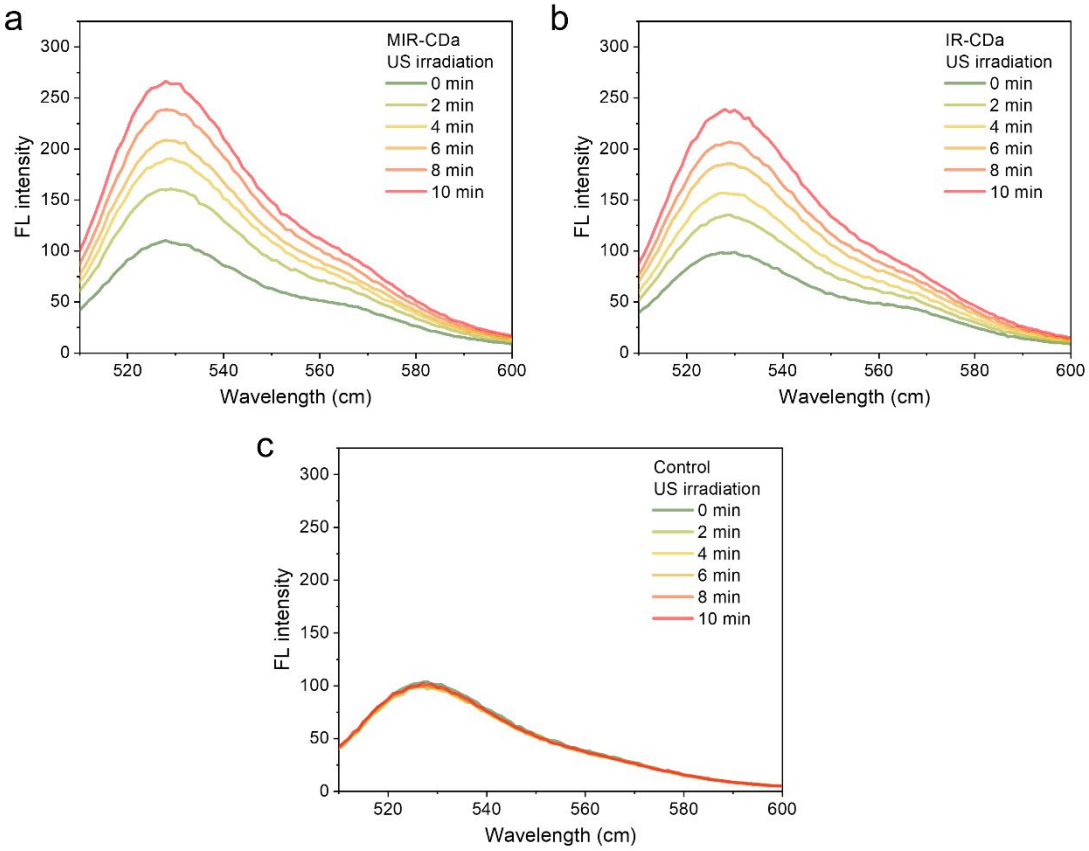


**Figure S8.** SOSG assay for $^1O_2$ generation ability under US irradiation (0.5 W cm$^{-2}$). a) MIR-CDa. b) IR CDa. c) Control. FL: Fluorescence.

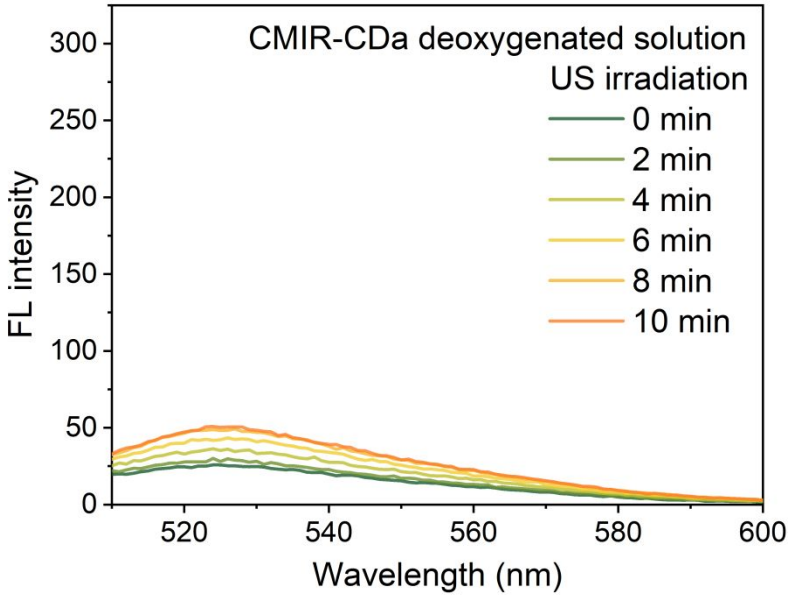


**Figure S9.** SOSG assay for $^1O_2$ generation ability of CMIR-CDa under US irradiation (0.5 W cm$^{-2}$) in deoxygenated solution. FL: Fluorescence.

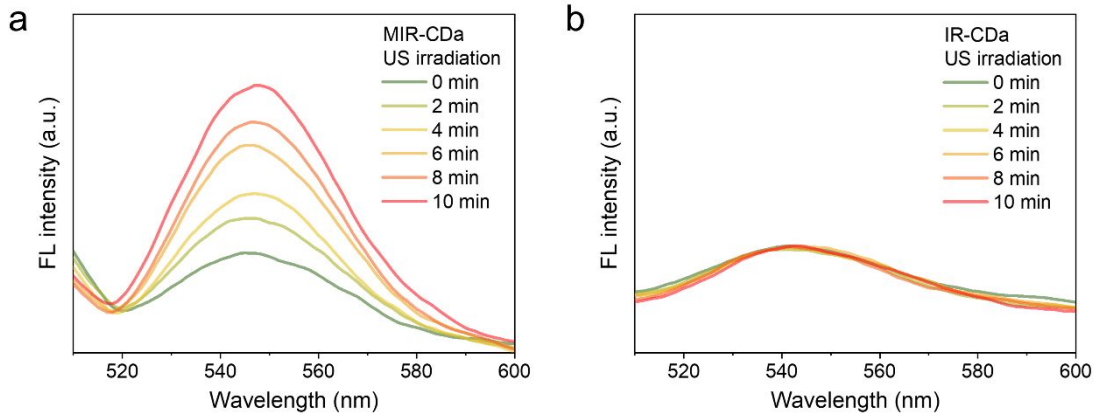


**Figure S10.** DHR 123 assay for $O_2^{\bullet-}$ generation ability under US irradiation (0.5 W $cm^{-2}$). a) MIR-CDa. b) IR CDa. FL: Fluorescence.

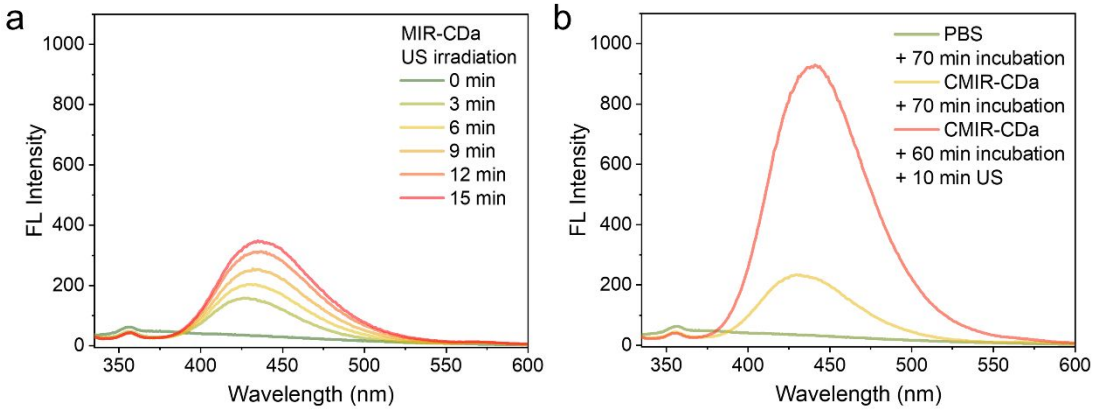


**Figure S11.** Terephthalic assay for •OH generation ability under US irradiation (0.5 W $cm^{-2}$). a) MIR-CDa. b) Comparison of •OH generation with and without US irradiation for CMIR-CDa. FL: Fluorescence.

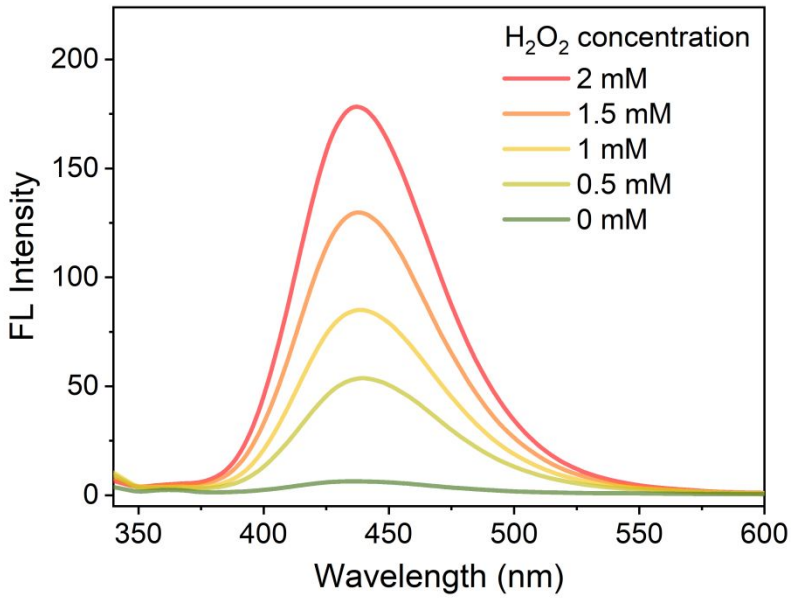


**Figure S12.** Terephthalic assay for •OH generation ability of CMIR-CDa under US irradiation (0.5 W $cm^{-2}$) with different $H_2O_2$ concentrations.

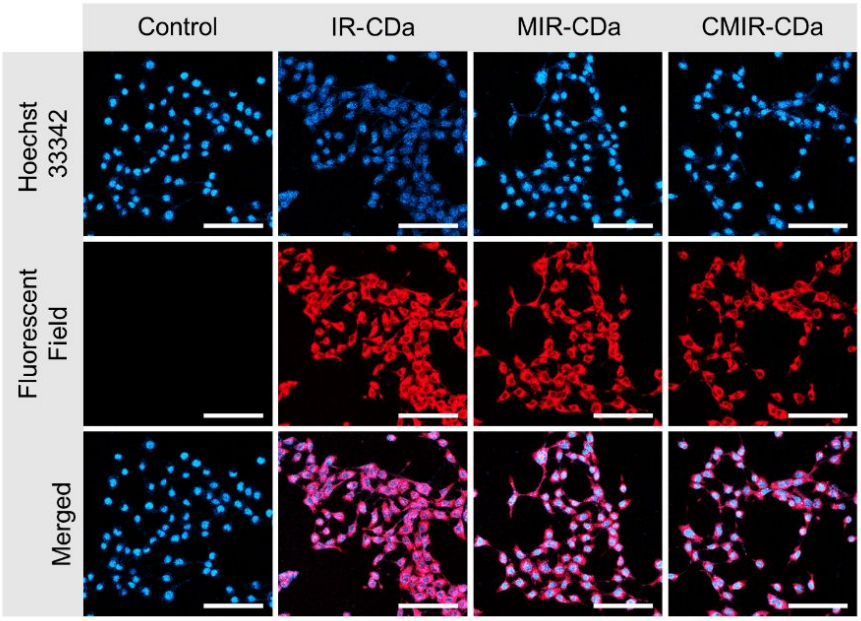


**Figure S13.** Confocal fluorescence imaging of 4T1 cells upon the incubation with IR-CDa, MIR-CDa, or CMIR-CDa. Scale bar is 100 μm.

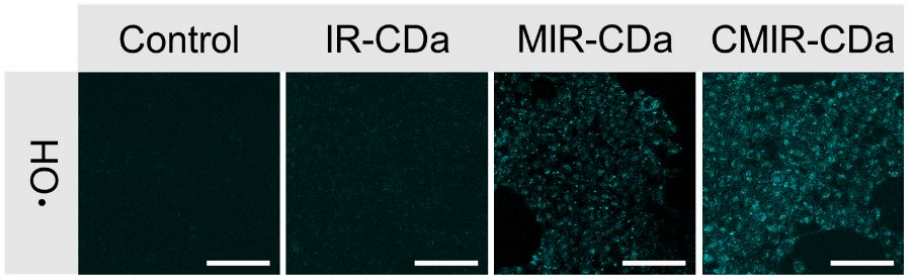


**Figure S14.** Intracellular •OH generation with US irradiation (3 min, 0.5 W $cm^{-2}$) detected by the coumarin-3-carboxylic acid assay. Blue fluorescence represents the •OH signal. Scale bar is 100 μm.

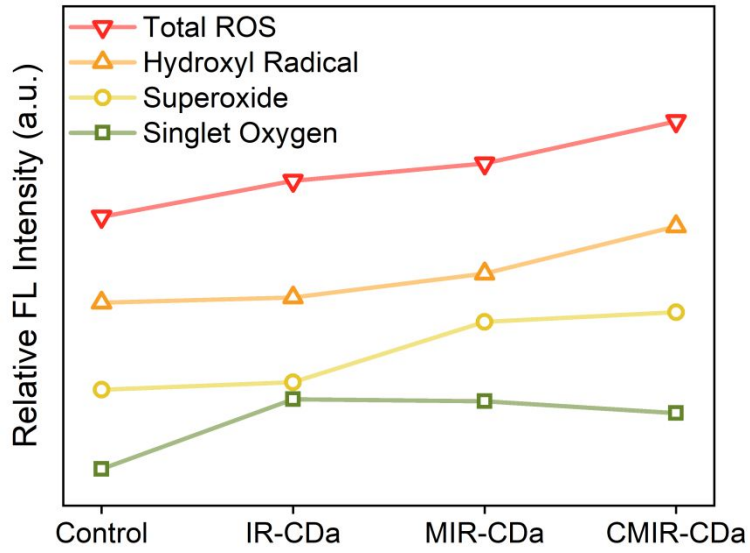


**Figure S15.** Relative fluorescence intensity derived from the CLSM images of different ROS assays for different groups indicated. FL: Fluorescence.

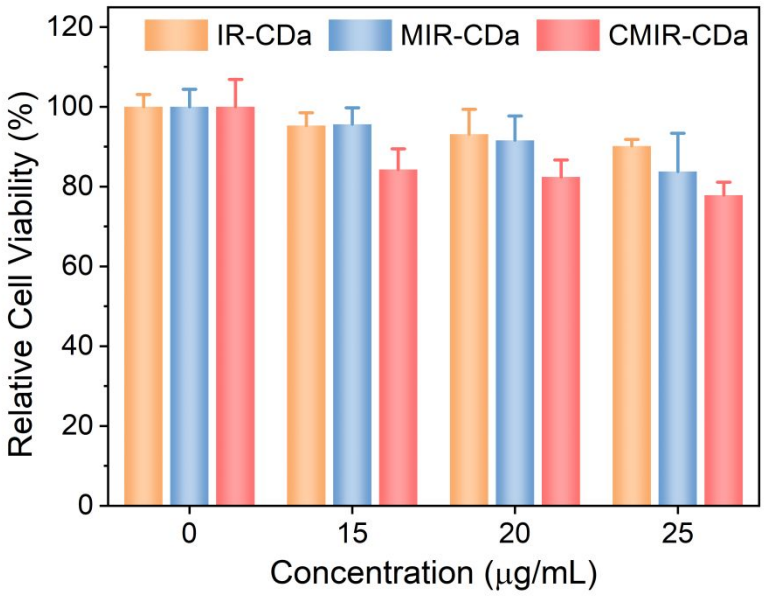


**Figure S16.** Concentration-dependent cytotoxicity of IR-CDa, MIR-CDa, and CMIR-CDa on 4T1 cells for 24 h determined by MTT assay (n = 5).

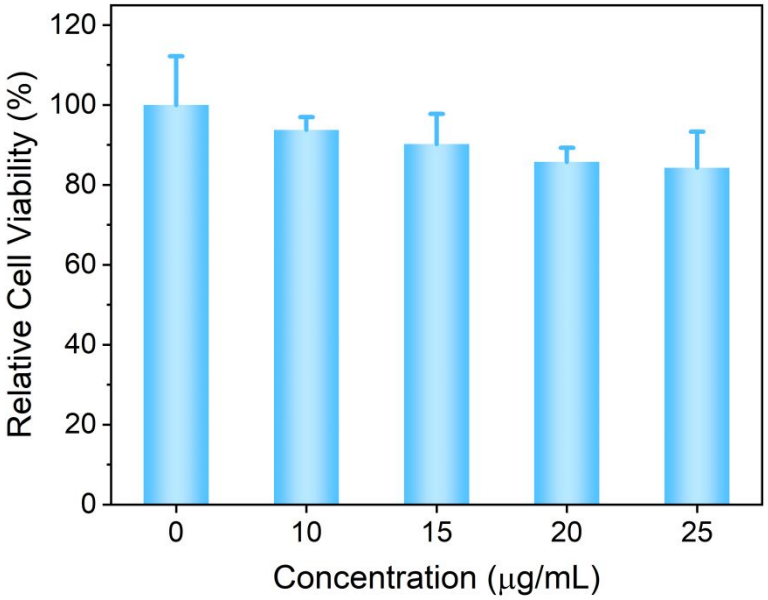


**Figure S17.** Concentration-dependent cytotoxicity of CMIR-CDa on HEK293 cells for 24 h determined by MTT assay (n = 5).

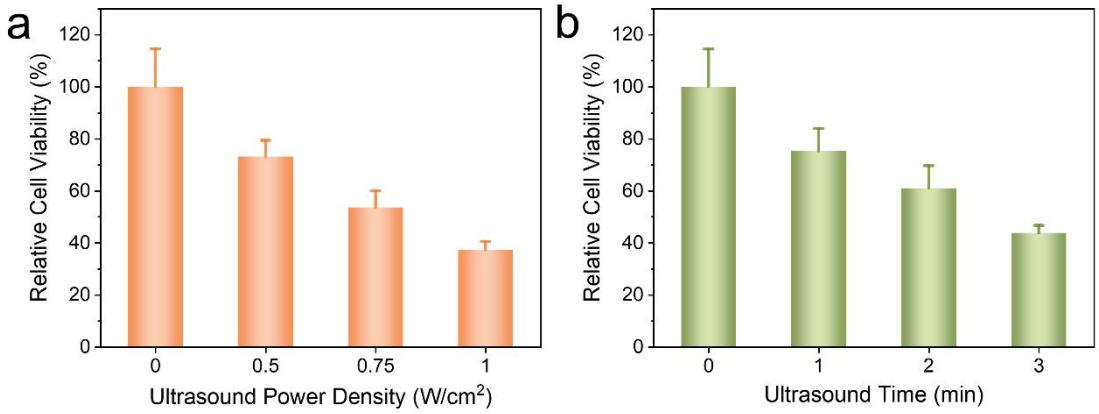


**Figure S18.** a) Ultrasound power density-dependent cytotoxicity of CMIR-CDa (irradiation time = 2.5 min) on 4T1 cells for 24 h determined by MTT assay (n = 4). b) Ultrasound irradiation time-dependent cytotoxicity of CMIR-CDa (power density = 0.75 W $cm^{-2}$) on 4T1 cells for 24 h determined by MTT assay (n = 4).

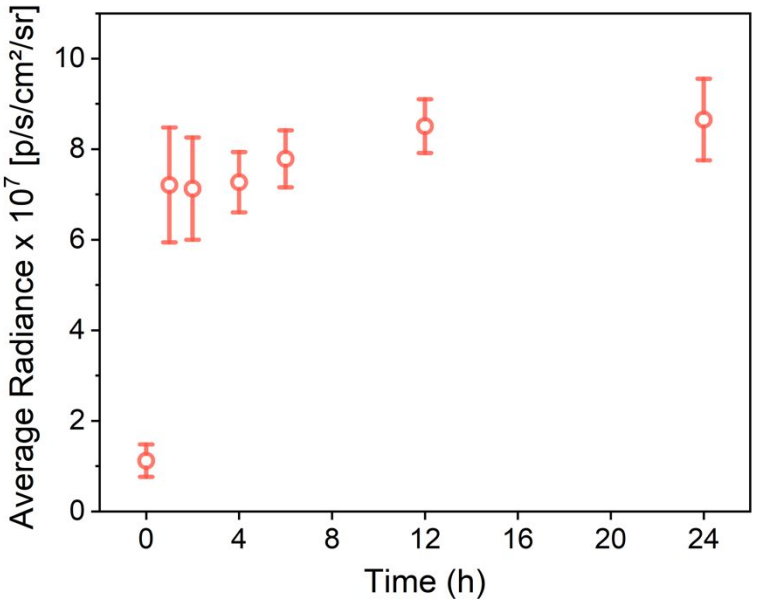


**Figure S19.** Quantification of *in vivo* fluorescence images for 4T1 tumor-bearing mice at the tumor region at different timepoints after the intravenous injection of CMIR-CDa.

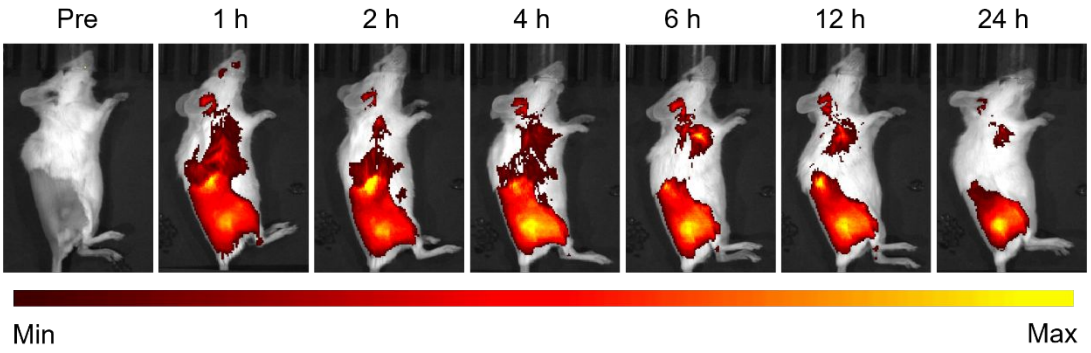


**Figure S20.** NIR fluorescence imaging of 4T1-tumor-bearing BALB/c mice at different timepoints after the intravenous injection of IR-CDa.

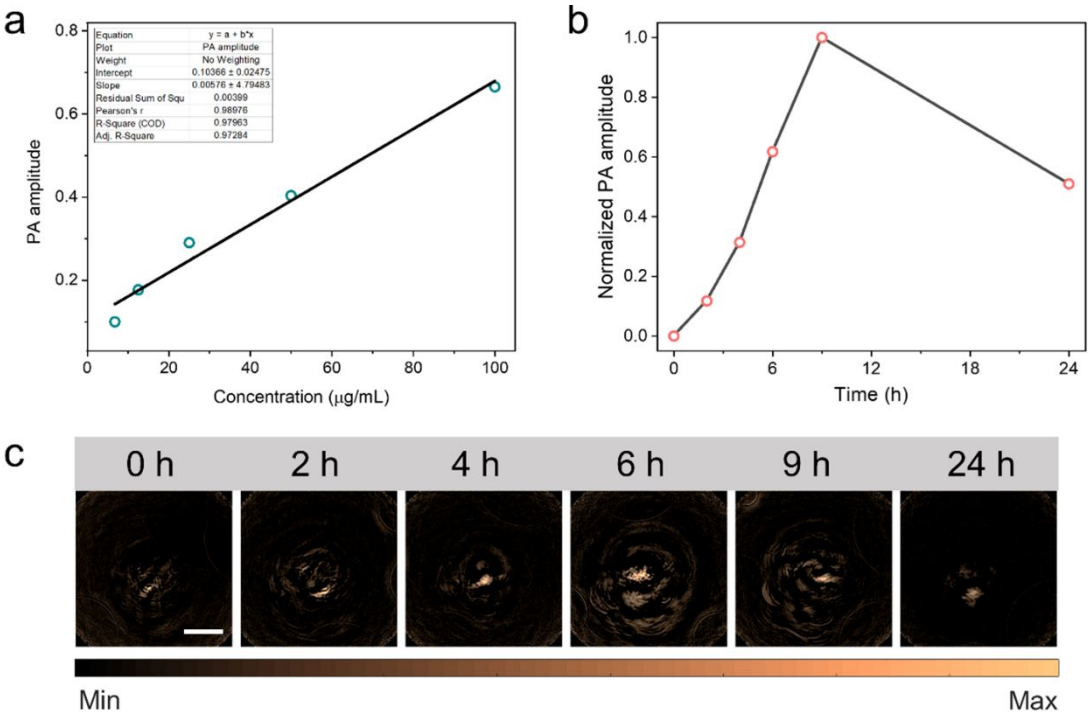


**Figure S21.** Photoacoustic tomography of CMIR-CDa. a) Linear fit of photoacoustic amplitudes of CMIR-CDa ($R^2$ = 0.97963) as a function of concentration at 700 nm. b,c) Time-course NIR-I photoacoustic tomography of tumor region on living mice bearing 4T1-xenograft tumor after intravenous administration of CMIR-CDa and quantification of photoacoustic amplitudes. Wavelength: 700 nm. Scale bar is 1 cm.

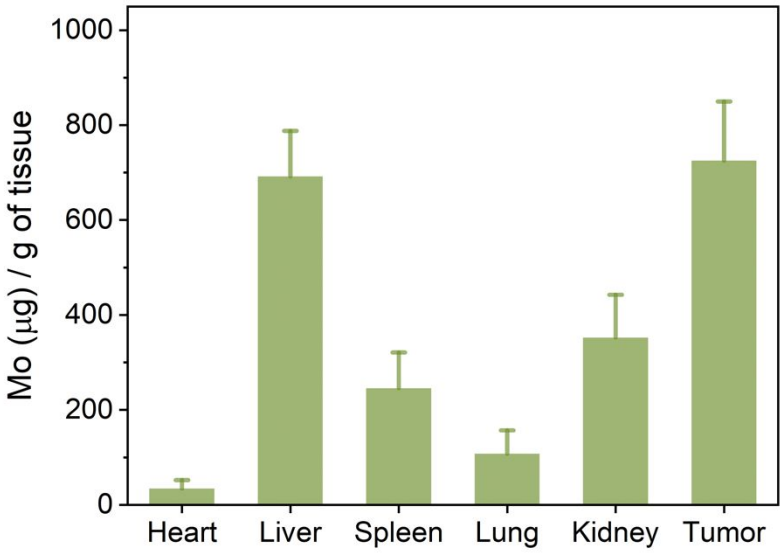


**Figure S22.** Distribution of Mo in the major organs (heart, liver, spleen, lung, and kidney) and tumor of 4T1 tumor-bearing mice after CMIR-CDa treatment for 24 h (n = 3).

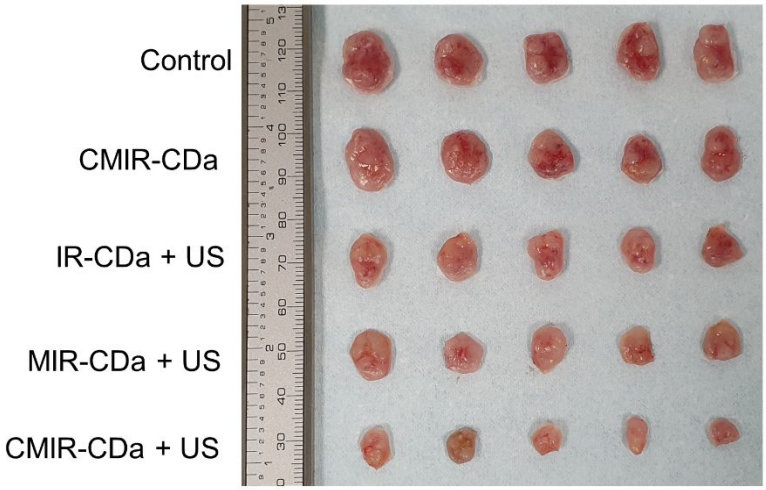


**Figure S23.** Photos of the excised tumors from different treatment groups after 14 days.

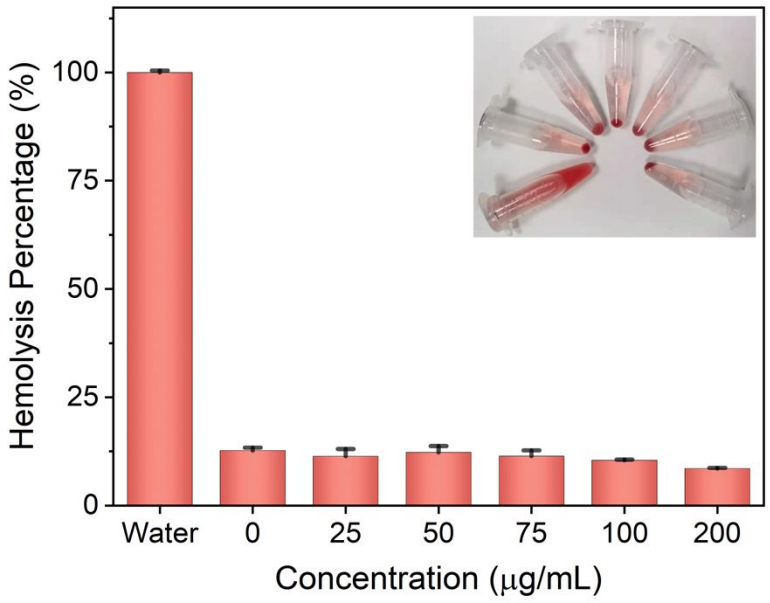


**Figure S24.** Hemolysis of CMIR-CDa at various concentrations. Inset: visual representation of centrifuged solutions to detect the presence of hemoglobin in supernatants.

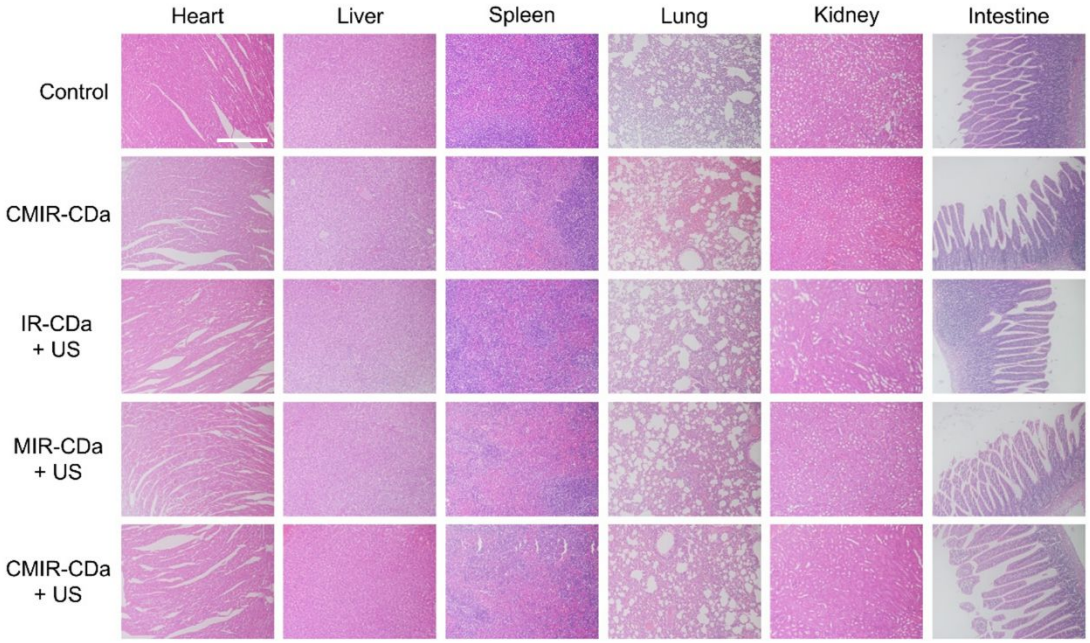


**Figure S25.** H&E staining of the main organs from the groups after the indicated treatments. Scale bar is 200 μm.